

1

2 **Genetics of white color and iridophoroma in “Lemon Frost” leopard geckos**

3

4 Longhua Guo^{1,*}, Joshua Bloom¹, Steve Sykes², Elaine Huang³, Zain Kashif¹, Elise Pham¹,
5 Katarina Ho¹, Ana Alcaraz⁴, Xinshu Grace Xiao³, Sandra Duarte-Vogel⁵, Leonid Kruglyak^{1,*}

6

7 ¹Department of Human Genetics, Department of Biological Chemistry, Howard Hughes Medical
8 Institute, University of California, Los Angeles, CA 90095, USA

9 ²Geckos Etc. Herpetoculture, Rocklin, CA 95765, USA

10 ³Department of Integrative Biology and Physiology, University of California, Los Angeles, CA
11 90095, USA

12 ⁴College of Veterinary Medicine, Western University of Health Sciences, Pomona, CA 91711,
13 USA

14 ⁵Division of Laboratory Animal Medicine, David Geffen School of Medicine, University of
15 California, Los Angeles, CA 90095, USA

16

17

18 (*) To whom correspondence should be addressed: longhuaguo@mednet.ucla.edu;
19 lkruglyak@mednet.ucla.edu

20

21 **Abstract**

22 The squamates (lizards and snakes) are close relatives of birds and mammals, with more than
23 10,000 described species that display extensive variation in a number of important biological
24 traits, including coloration, venom production, and regeneration. Due to a lack of genomic tools,
25 few genetic studies in squamates have been carried out. The leopard gecko¹, *Eublepharis*
26 *macularius*, is a popular companion animal, and displays a variety of coloration patterns. We

27 took advantage of a large breeding colony and used linkage analysis, synteny, and
28 homozygosity mapping to investigate a spontaneous semi-dominant mutation, “Lemon Frost”,
29 that produces white coloration and causes skin tumors (iridophoroma). We localized the
30 mutation to a single locus which contains a strong candidate gene, SPINT1^{2,3}, a tumor
31 suppressor implicated in human skin cutaneous melanoma (SKCM) and over-proliferation of
32 epithelial cells in mice and zebrafish⁴⁻¹⁶. Our work establishes the leopard gecko as a tractable
33 genetic system and suggests that a tumor suppressor in melanocytes in humans can also
34 suppress tumor development in iridophores in lizards.

35

36 **Introduction**

37 Color-producing cells¹⁻⁵ contribute to animal coloration and patterns. Some cells, such as
38 melanocytes, produce pigments chemically. Others, such as iridophores, produce colors
39 structurally by making crystal platelets⁶⁻⁹. Iridophores are not present in mammals, but are
40 widespread in insects, fish, birds, amphibians and reptiles. Different types of iridophores can
41 lead to different colors, including blue^{10,11} and white¹². There have been few molecular genetic
42 analyses of the regulation of chromatophores in cells other than melanocytes. A recent study
43 found that endothelin signaling regulates iridophore development and proliferation in zebrafish¹³.
44 In mammals, this pathway is required for melanocyte development¹⁴, suggesting that signaling
45 pathways conserved in evolution can be adapted to regulate different types of chromatophores.

46

47 Many reptile species (e.g., geckos, chameleons, snakes) are bred in captivity as companion
48 animals, and breeders have established morphs with unique colors and patterns². The
49 inheritance of different color morphs is usually carefully documented by breeders. The common
50 leopard gecko, *Eublepharis macularius*, is an especially attractive model to study the molecular
51 regulation of coloration because dozens of color and pattern morphs have been established
52 over the past 30 years of selective breeding. These morphs either intensify a particular color

53 (Supplementary Figure1 A-I) or rearrange coloration patterns (Supplementary Figure1 J-L). A
54 draft leopard gecko genome assembly has been published, containing 2.02 Gb of sequence in
55 22,548 scaffolds, with 24,755 annotated protein-coding genes¹⁵. Embryonic development *in ovo*
56 and blastema-based tail regeneration have also been staged and documented in great detail¹⁶⁻¹⁸.
57 Here, we took advantage of these established resources and used quantitative genetics to gain
58 insight into the molecular regulation of white color in leopard geckos.

59

60 **Results**

61

62 **The Lemon Frost allele is a spontaneous semidominant mutation**

63 A spontaneous mutation occurred in a female hatchling from a cross between two wildtype
64 leopard geckos. This mutation increased the white color of the leopard gecko, resulting in
65 brightened white and yellow colors. This unique color morph was named Lemon Frost¹⁹ (Figure
66 1). A male leopard gecko carrying the *lemon frost* (*lf*) allele, Mr. Frosty (Figure 1B), was crossed
67 to 12 female leopard geckos of different genetic backgrounds. The F1 progeny, which were
68 heterozygous for the *lf* allele, were backcrossed to the same maternal lines or intercrossed to
69 establish a colony of more than 900 animals (Supplementary Figure 2). Homozygous F2
70 intercross progeny were named super Lemon Frost (Figure 1C). These homozygous mutants
71 have an accentuated color phenotype and thickened skin, which is most apparent in their
72 eyelids (Figure 1C, red arrow). Heterozygous Lemon Frost animals were also crossed to
73 another mutant, Blizzard, which is light yellow without other colors or patterns (Figure 1D). The
74 homozygous Blizzard progeny carrying the *lf* allele displayed excessive white color in their
75 heads and trunks, which brightened Blizzard's yellow color (Figure 1E). The *lf* allele also
76 increased white color in the retina (Figure 1E). The segregation pattern of Lemon Frost in
77 pedigrees is consistent with single-locus Mendelian inheritance (Figure 1F-H). The *lf* allele is

78 semidominant, as homozygous mutants have more pronounced phenotypes than do
79 heterozygotes (Figure 1B-C and F-H).

80

81 **The *lemon frost* allele leads to iridophoroma, with potential metastasis in homozygous**
82 **animals**

83 Heterozygous Lemon Frost mutants were recently reported to develop iridophoroma¹⁹, a tumor
84 of iridophores. Histopathological examination of the skin samples from homozygous mutants,
85 with accentuated phenotypes, showed large solid sheaths of round to polygonal neoplastic cells
86 that efface and expand the normal tissue architecture (Supplementary Figure 3). The cells have
87 abundant cytoplasm with bright brownish intracytoplasmic pigment. The nuclei are eccentric and
88 vary from round to fusiform. The white tumor masses stain dark with Hematoxylin and Eosin
89 (H&E), and remain brightly reflective under dark-field illumination (Supplementary Figure 4A,B),
90 consistent with their nature as iridophores^{10,20-23}. Imaging with Transmission Electron
91 Microscopy (TEM) showed that the *If* allele led to both increased numbers of neoplastic
92 iridophores and increased production of reflective platelets within each iridophore²⁴
93 (Supplementary Figure 4C). In addition to skin, other affected organs in homozygous mutants
94 include liver, eye, and muscle. The interpretation of the widespread neoplastic nodules is that
95 the tumors are malignant iridophoroma.

96

97 More than 80% of both male and female animals carrying the *If* allele developed white tumors 6
98 months to 5 years after birth. The tumors manifest as patches of white cells in the skin, which
99 are most evident on the ventral side of the animal (Figure 2A). The tumor skin can be severely
100 thickened and leathery (Figure 2B, Supplementary Figure 3). It is resistant to liquid nitrogen
101 freezing, or to Dounce homogenization, making RNA extraction infeasible. In severe cases in
102 heterozygous mutants, the tumors develop into skin protrusions (Figure 2C, left), which contain

103 dense white masses (Figure 2C, right). Tumors cover a greater fraction of the skin of
104 homozygous mutants. Surprisingly, these tumors rarely develop into skin protrusions as in
105 heterozygous animals. Instead, they manifest as well-demarcated, white, thickened patches on
106 the ventral skin (Figure 2A), thickened layers of white masses all over the dorsal skin (Figure
107 2B), white, multifocal, variably sized, well-demarcated nodules in the liver, and patches of white
108 cells in the oral cavity (Figure 2D).

109

110 **Linkage and association analysis in a breeding pedigree**

111 To identify the genetic locus that regulates white color and tumor growth in *Lemon Frost*
112 mutants, we used restriction site-associated DNA sequencing (RAD-Seq) to genotype 188
113 animals from the breeding pedigree (Figure 3, Supplementary Figure 2), including 33 super
114 Lemon Frost (*lfl/lfl*), 116 Lemon Frost (*lfl/+*), and 39 wild-type (*+/+*) individuals. We identified a
115 total of 14,857 variants covering 2,595 scaffolds of the genome assembly. To map the Lemon
116 Frost locus, we tested the effect of allelic dosage at each marker on white coloration of the
117 geckos in a standard semi-dominant association mapping framework, accounting for population
118 structure through the use of marker-based relatedness. We used a p-value threshold of 7.09e-5
119 (Methods) to control the false positive rate at 1%. Forty-eight markers on 31 scaffolds were
120 significantly associated with white coloration (Supplemental Table). The top two association
121 signals corresponded to scaffolds 6052 and 996.

122

123 **Synteny analysis and homozygosity mapping**

124 Because the gecko genome assembly is highly fragmented, we used synteny to examine
125 whether the 31 scaffolds associated with coloration belong to a single genomic interval. We
126 compared the gecko scaffolds to homologous regions of the most closely related species with
127 chromosome-scale genome assemblies: chicken²⁵ and human²⁶. We found that 17 out of 22
128 scaffolds that have synteny information (including scaffolds 6052 and 996) correspond to one

129 region on chicken chromosome 5 and human chromosome 15 (Figure 3A-C, Supplemental
130 Table). The 28 markers on these 17 scaffolds are in linkage disequilibrium (Figure 3B), which
131 decays with distance when markers are ordered by synteny (Figure 3B). These results indicate
132 that a single genomic region is associated with the Lemon Frost phenotype, as expected for a
133 new mutation with a Mendelian segregation pattern.

134
135 To narrow down the location of the causal gene within this genomic region, we used whole
136 genome sequencing and homozygosity mapping. We pooled DNA from 25 super Lemon Frost
137 genomes (*lfl/lfl*), 63 Lemon Frost genomes (*lfl/+*), and 71 wildtype geckos (*+/+*) and sequenced
138 each pool to 30x coverage. We reasoned that the *lfl* mutation in Mr. Frosty and its flanking
139 variants should form a haplotype that would be found in the super Lemon Frost pool with 100%
140 frequency, in the Lemon Frost pool with 50% frequency, and would not be seen in the wildtype
141 pool. We scanned the genome in 10 kb windows and measured the fraction of heterozygous
142 variants from Mr. Frosty that followed this expected pattern in the pools. This statistic was
143 highest for a window on scaffold 996 (Supplementary Table, Methods), the main candidate
144 scaffold from statistical mapping. The expected frequency pattern was observed for 20 of 22
145 variants in this window (630-640kb on scaffold 996). Four of the top six intervals fall in the
146 region from 570kb to 640kb on scaffold 996, with the signal decaying with distance away from
147 this region (Figure 3D,E). The linkage between this region and Lemon Frost was replicated in an
148 independent 3-generation backcross between Mr. Frosty and a Sunburst Tangerine morph
149 (Figure 4). These results indicate that scaffold 996 contains the Lemon Frost mutation.

150

151 **SPINT1 is a strong candidate gene for the Lemon Frost phenotype**

152 The genomic interval spanning positions 570kb-640kb on scaffold 996 contains a single gene,
153 SPINT1. SPINT1 (serine peptidase inhibitor, Kunitz type 1), also known as hepatocyte growth
154 factor activator inhibitor type 1 (HAI-1), is a transmembrane serine protease inhibitor expressed

155 mainly in epithelial cells²⁷⁻²⁹. It is the only gene in the larger associated region reported to be a
156 suppressor of epithelial cell tumors in model organisms and in humans^{27,30-41}. Because the
157 breeding and transmission data indicate that the *If* allele arose from a single spontaneous
158 mutation, we reasoned that a mutation disrupting SPINT1 causes the over-proliferation of white-
159 colored skin cells in Lemon Frost geckos.

160

161 The Lemon Frost SPINT1 allele differs from the reference genome assembly at two positions in
162 the exons, as well as at 147 positions in the introns and the 3'UTR (Supplemental Table). This
163 large number of variants is a consequence of differences in genetic background between Mr.
164 Frosty's parents and the non-Lemon Frost individual used to generate the reference, and makes
165 it challenging to identify the causal mutation. Both differences in the coding sequence of
166 SPINT1 are synonymous. Notable differences in non-coding regions include 7 large
167 insertion/deletions (indels) in the introns and a 13-nucleotide insertion in the 3'UTR
168 (CAAGTGTATGTAT). Indels in introns and promoters of SPINT1 have been reported to lead to
169 loss of SPINT1 function in fish and mice^{36,37,41}.

170

171 Sequencing of RNA extracted from normal gecko skin and from skin peripheral to tumors in
172 homozygous mutants confirmed that SPINT1 is expressed in this tissue (Supplemental Figure
173 5). However, we did not observe a significant difference between homozygous mutants and
174 wildtype geckos in SPINT1 mRNA levels or splicing patterns. This result suggests that the
175 putative causal mutation in SPINT1 may alter translation or protein activity, rather than
176 transcription. Alternatively, the mutation might reduce SPINT1 expression only in tumors, which
177 are refractory to RNA extraction as noted above.

178

179 **Discussion**

180 Several lines of evidence support our hypothesis that a defect in SPINT1 causes iridophoroma
181 in Lemon Frost geckos. First, SPINT1 function is dosage-dependent, consistent with our
182 observation that Lemon Frost is a semi-dominant phenotype. In humans, carcinoma tissues *in*
183 *vivo* and carcinoma-derived cell lines *in vitro* have reduced SPINT1 on the cell membrane^{42,43}
184 through enhanced shedding of the extracellular domain or decreased mRNA or protein
185 expression. Reduced expression of SPINT1 has been associated with a negative prognosis of
186 human Skin Cutaneous Melanoma (SKCM)³⁰ and pancreatic ductal adenocarcinoma³¹.
187 Knockdown of SPINT1 expression by siRNA in cancer cell lines led to increased invasion or
188 metastasis^{32,43,44}. Second, loss of SPINT1 function in fish and mice leads to tumor formation in
189 epithelial cells. In mice, homozygous deletion of SPINT1 leads to disrupted placental basement
190 membranes and embryonic lethality^{37,39}. Rescued mosaic animals developed scaly skin with
191 hyperkeratinization⁴⁰. Intestine-specific deletion of SPINT1 leads to increased tumor growth of
192 intestine epithelium³³. Increased expression of SPINT1 in the skin abrogated matriptase-
193 induced spontaneous skin squamous cell carcinoma⁴⁵. In zebrafish, reduced expression led to
194 hyperproliferation of basal keratinocytes³⁶ and enhanced proliferation of epithelial cells⁴¹.
195 Furthermore, SPINT1 deficiency was used to establish a disease model for Skin Cutaneous
196 Melanoma (SKCM) in zebrafish³⁰. In all three studies in zebrafish, skin inflammation was
197 observed. Third, insertions in introns^{36,37} and promoters⁴¹ have caused loss of SPINT1 function.
198 Together with our genetic localization of the *lf* locus to SPINT1, these lines of evidence make
199 this gene a very strong candidate for the Lemon Frost phenotype.

200

201 Molecular genetics in reptiles is not well established due to long reproductive cycles and
202 challenges in laboratory breeding. Early work focused on careful documentation of patterns of
203 inheritance^{2,46}. Molecular studies have examined sequence variants in a candidate pigmentation
204 gene, melanocortin-1 receptor, and their association with melanic or blanched phenotypes in
205 different species and ecological niches⁴⁷⁻⁵⁴. Recently, CRISPR-Cas9-mediated gene editing was

206 successfully used to mutate the tyrosinase gene in the lizard *Anolis sagrei*⁵⁵. Although this
207 species is only distantly related to the leopard gecko, this advance offers promise that targeted
208 studies of the role of SPINT1 mutations in the Lemon Frost phenotype will become possible.

209

210 White iridophoroma is common in many reptile species⁵⁶, including green iguanas⁵⁷, captive
211 snakes⁵⁸, bearded dragons⁵⁹ and veiled chameleons⁶⁰. The genetic causes of this phenotype in
212 these species are unknown. Most of our knowledge about molecular and cellular regulation of
213 iridophores derives from work in zebrafish^{11-13,61-71}. Interestingly, few cases of iridophoroma
214 have been reported in zebrafish⁷². We found that an evolutionarily conserved gene, SPINT1,
215 regulates the proliferation of white iridophores in the leopard gecko. The tumor suppressor
216 function of SPINT1 establishes a link between iridophoroma and regulation of white coloration in
217 reptiles. Our work suggests that cancer genes can play as important a role in iridophores as
218 they do in melanocytes and melanoma⁷³, and that Lemon Frost leopard geckos can serve as a
219 disease model to study Skin Cutaneous Melanoma.

220

221 **Methods**

222

223 Gecko maintenance and experimental procedures

224

225 All activities involving animals included in this manuscript were approved by the University of
226 California, Los Angeles (UCLA) Institutional Animal Care and Use Committee. Leopard geckos
227 were acquired from a commercial breeder. Housing conditions at UCLA included: room
228 temperature of 70-80 F, cage temperature of 72-95 F, room relative humidity between 30-60%,
229 and a 12:12 hours light cycle. A heating pad was provided at one side of the cage to establish a
230 temperature gradient. Animals were singly housed in polycarbonate cages with cardboard lines
231 (Techboard[®]) at the bottom, water was provided in bowls inside the cage, and PVC pipe pieces

232 and plastic plants were offered as environmental enrichment. Geckos were fed 2-6 fresh
233 crickets and 2-4 mealworms three times per week.

234

235 Geckos were euthanized with an intracoelomic injection of sodium pentobarbital (Euthasol[®]) at
236 a dose of 100-200 mg/Kg. Immediately after euthanasia, a necropsy was performed, including
237 external examination, body and organ weighing, gross assessment of normal and abnormal
238 tissues, and tissue collection for histopathology processing and assessment. Normal and
239 abnormal tissues were fixed in 10% formalin, embedded in paraffin, sectioned, and stained with
240 H&E for pathologic evaluation.

241

242 Phenotyping

243

244 Lemon Frost and super Lemon Frost phenotypes were determined according to a list of rules,
245 based on increased white color of the body, eye, and belly compared to normal wildtype animals
246 (http://www.geckosetc.com/lemon_frost_info.html). Pictures were taken for each animal to
247 document the phenotype.

248

249 Genotyping

250

251 Genomic DNA was extracted from fresh tail tips with Easy-DNA gDNA purification kit (K180001,
252 ThermoFisher), or from the saliva with PERFORMAgene (PG-100, DNAgenotek). Genomic
253 DNA extracted from saliva was further purified with ethanol precipitation before genotyping
254 assays. DNA libraries for whole genome sequencing were prepared with Nextera DNA Library
255 Prep Kit (FC-121-1031, Illumina). Libraries for RADseq were prepared according to the

256 procedures of Adapterama III⁷⁴ with few modifications. Libraries were sequenced on a HiSeq
257 3000 (Illumina).

258

259 Only scaffolds larger than 5kb in the draft genome assembly were used as a reference. RADseq
260 reads and Whole Genome Sequencing (WGS) reads were aligned to the leopard gecko draft
261 genome¹⁵ with bwa mem⁷⁵. Variants for WGS were identified with GATK⁷⁶. Variants for RADseq
262 were identified with Stacks^{77,78}. All variants were filtered with VCFtools⁷⁹. Only high-quality
263 variants were used in homozygosity mapping or statistical mapping (DP>=30, GQ>=30).

264

265 Transcriptome sequencing

266

267 Skin tissue samples around 6mm in diameter were taken from the ventral side of the geckos
268 after anesthetization with 1-5% isoflurane. As tumor tissues are refractory to RNA extraction,
269 flanking tumor-free tissue samples were taken for homozygous Lemon Frost animals. All
270 samples were homogenized with TissueRuptor in buffer RLT immediately after collection.
271 Lysates were immediately frozen on dry ice until all tissues were collected from animals. Then
272 all lysates were centrifuged for 5 minutes at 13,000 rpm to remove debris. Supernatants were
273 taken to fresh tubes, and mRNA was extracted according to the procedures of RNeasy Fibrous
274 Tissue Mini Kit (74704, QIAGEN).

275

276 Libraries of extracted mRNA were prepared with RNA HyperPrep kit (KAPA) and sequenced on
277 a HiSeq 3000 (Illumina). RNA-seq reads were mapped to the leopard gecko draft genome¹⁵
278 using HISAT2 with default parameters. Identification of alternative and differential splicing
279 events was performed using JuncBase⁸⁰. Gene expression was compared using Sleuth⁸¹ after
280 RNA transcript abundance was quantified using Kallisto⁸².

281

282 Pathology

283

284 Complete postmortem examination was performed, and representative tissue samples were
285 obtained. All tissues obtained at necropsy were preserved in 10% neutral-buffered formalin
286 solution for up to 5 days before being processed and embedded in paraffin. All tissues were
287 sectioned at 5 μ m, and routinely stained with Hematoxylin and Eosin.

288

289 Statistical Mapping

290

291 Biallelic markers with minor allele frequency of less than 5% and with fewer than 10 individuals
292 called as homozygous for both the reference and alternative alleles were excluded from
293 mapping and kinship matrix construction. A kinship matrix was calculated using the function
294 *A.mat* with default parameters from the rrBLUP⁸³ R package. Phenotype was encoded as 0 for
295 wild type, 1 for Lemon Frost, and 2 for super Lemon Frost. Association statistics between this
296 phenotype vector and marker genotypes were computed using the function *gwas2* in the NAM⁸⁴
297 R package using a linear mixed model with a random effect of kinship to control for population
298 structure. The effective number of tests was computed to be 141.1 based on the procedure of
299 Galwey et al⁸⁵. A family-wise error rate significance threshold was calculated as 0.01/141.1 or
300 $p < 7.09e-5$.

301

302 Homozygosity Mapping

303

304 Pooled animals and Mr. Frosty were sequenced to ~30x coverage on a HiSeq 3000 (Illumina).
305 Variants were identified with GATK and filtered with VCFtools. Biallelic heterozygous variants
306 from Mr. Frosty, including indels, were used as markers to localize the Lemon Frost mutation.
307 Allele ratios (AF) were calculated by dividing the read count of alternative alleles by the sum of

308 the counts of reference alleles and alternative alleles. Variants closely linked to the Lemon Frost
309 mutation are expected to have AF between 0.4 and 0.6 in the Lemon Frost pool and in Mr.
310 Frosty, AF > 0.85 in the super Lemon Frost pool, and AF < 0.15 in the wildtype pool. The
311 number of variants meeting these criteria was counted for every 10kb genome interval. The
312 fraction of such variants among all variants heterozygous in Mr. Frosty within the interval was
313 then calculated. Intervals with fewer than 5 variants were excluded because they could not
314 provide statistically meaningful results.

315

316 Transmission Electron Microscopy

317

318 Dissected skin tissues were fixed in 2.5% glutaraldehyde and 4% formaldehyde in 0.1 M sodium
319 cacodylate buffer overnight at 4 °C. After being washed in PBS, samples were post-fixed in 1%
320 osmium tetroxide in 0.1M sodium cacodylate, and dehydrated through a graded series of
321 ethanol concentrations. After infiltration with Eponate 12 resin, the samples were embedded in
322 fresh Eponate 12 resin and polymerized at 60°C for 48 hours. Ultrathin sections of 70 nm
323 thickness were prepared, placed on formvar-coated copper grids, and stained with uranyl
324 acetate and Reynolds' lead citrate. The grids were examined using a JEOL 100CX transmission
325 electron microscope at 60 kV, and images were captured by an AMT digital camera (Advanced
326 Microscopy Techniques Corporation, model XR611).

327

328 **Acknowledgement**

329 We thank Aaron Miller, Jasmine Gonzalez, Kendall Placido and James Walter for their
330 assistance in gecko DNA collection and phenotyping. We thank members of the Kruglyak lab for
331 helpful feedbacks on the project, and Giancarlo Bruni, Stefan Zdraljevic, Eyal Ben-David and
332 Olga Schubert for helpful comments on the manuscript. We thank Chunni Zhu (Electron

333 Microscopy Core Facility, UCLA Brain Research Institute) for her assistance in TEM sample
334 processing and imaging. We thank Jonathan Eggenschwiler for helpful discussions.

335

336 This work is supported by the Howard Hughes Medical Institute (LK) and the Helen Hay
337 Whitney Foundation (LG).

338

339 **Figure legends**

340

341 **Fig 1 The Lemon Frost mutant of the common leopard gecko, *Eublepharis macularius*.** (A)
342 wild type; (B) heterozygous mutant; (C) homozygous mutant, with red arrow pointing to the eye
343 lid; (D) blizzard mutant with minimal color; (E) Lemon Frost mutation (*lf*) on the blizzard
344 background; (F-H) segregation of the *lf* allele. Lemon Frost (LF) denotes heterozygotes for the
345 mutation; super LF denotes homozygotes for the mutation. All proportions are consistent with
346 expectations for single-locus Mendelian inheritance (chi-square test $p > 0.1$).

347

348 **Fig 2 Tumor growth and metastasis in the Lemon Frost mutant.** Designations are
349 homozygous mutant (*lf/lf*); heterozygous mutant (*lf/+*); wild type (+/+). (A) tumors in ventral skin;
350 (B) thick layers of white tumor cells (*lf/lf*) vs. normal white cells (+/+); (C) outgrowth of white
351 tumor cells (*lf/+*); (D) metastasis of white tumor cells in the liver and oral cavity. Red arrows:
352 white colored tumor cells. Arrowhead in B: normal white cells.

353

354 **Fig 3 Localization of the Lemon Frost mutation.** (A) p-value for association with white color
355 and (B) linkage disequilibrium for 28 markers syntenic to chicken chromosome 15 (red, ordered
356 by synteny), 4 markers syntenic to chromosome 5 (cyan), and 16 markers without synteny
357 information (green). (C) A schematic of the region showing synteny and gene annotation. (D)
358 Fraction of markers showing expected allele frequency pattern in pools, plotted for 10kb
359 windows along scaffold 996. The four windows with the highest fraction are marked by asterisks
360 and span the location of the gene SPINT1. Windows with fewer than 5 variants were not plotted
361 (dashed red lines). (E) Genome-wide distribution of the fraction of markers showing expected
362 allele frequency pattern in pools for all 10 kb windows. The 4 highest windows on scaffold 996
363 (red arrows) marked in D are among the 6 highest windows in the entire genome.

364

365 **Fig 4 The *lemon frost* allele in a backcross.** (A) We genotyped 7 progeny with the Lemon
366 Frost phenotype and 6 wild type progeny from the third generation of a backcross of Mr. Frosty
367 to the Sunburst line for markers in the SPINT1 region and observed a consistent inheritance
368 pattern. (B) Sequencing chromatogram of a heterozygous animal (*lf/+*) at an insertion marker.
369 (C) Sequencing chromatogram of a homozygous animal (+/+) at the same insertion marker.

370

371 **SupFig 1 Coloration and pattern diversity of the common leopard gecko, *Eublepharis***
372 ***macularius*.** (A) wild type; (B) black night; (C) variant of black night; (D) granite snow; (E) gem
373 snow; (F) white knight; (G) sunburst tangerine; (H-I) variants of sunburst tangerine; (J) red
374 stripes; (K) bold stripes; (L) rainbow.

375

376 **SupFig 2 Breeding pedigree of the Lemon Frost mutation.** Mr. Frosty, the original carrier of
377 the spontaneous Lemon Frost mutation, was bred to 12 female geckos from different genetic

378 backgrounds. F1s carrying the *lf* allele were bred among themselves or back to their female
379 parent, producing the second generation of animals heterozygous or homozygous for the *lf*
380 allele. Blue: *lf/lf*; green: *lf/+*; red: *+/+*. Dashed line: same individual/line.

381

382 **SupFig 3 Histopathology of skin tumors.** (A) Thick layers of white tumor tissue (star)
383 infiltrating white skin (arrow). (B) Skin biopsies organized and fixed in a paper roll for sectioning.
384 (C) H&E staining of the skin sections. Arrow: skin; star: infiltrated tumor mass. (D) H&E staining
385 of the skin sections showing normal skin cells and neoplastic cells (star). Neoplastic cells have
386 eccentric and condensed nuclei.

387

388 **SupFig 4 Potential metastasis of iridophoroma.** (A) In normal skin, cell nuclei are oval and
389 perpendicular to the skin surface. In Lemon Frost skin, cell nuclei are flat, elongated and parallel
390 to the skin, reminiscent of epithelial-to-mesenchymal transition. (B) Iridophoroma in the liver,
391 stained dark in H&E sections. In dark field imaging, iridophores are bright white. Such
392 iridophores invade blood vessels in the tissue (red arrows). (C) In TEM imaging, white tumor
393 skins in super LF are filled with abundant iridophores with excessive brightly reflective crystals
394 (Tumor). In normal skin, iridophores are much fewer and have less crystals (Normal).

395

396 **SupFig 5 SPINT1 expression in gecko skin.** SPINT1 mRNA reads from transcriptome
397 sequencing were aligned to the genome and visualized in IGV. Top 3 rows show samples from
398 homozygous mutants. Bottom 3 rows show samples from wild type geckos. Skin tissue adjacent
399 to the tumors was used in the mutants. Peaks mark SPINT1 exons. The last exon on the right is
400 transcribed together with the 3'UTR.

401

402

403 References

404

- 405 1 Fujii, R. in *International Review of Cytology* Vol. 143 (eds Kwang W. Jeon, Martin
406 Friedlander, & Jonathan Jarvik) 191-255 (Academic Press, 1993).
- 407 2 Olsson, M., Stuart-Fox, D. & Ballen, C. Genetics and evolution of colour patterns in
408 reptiles. *Seminars in Cell & Developmental Biology* **24**, 529-541,
409 doi:<https://doi.org/10.1016/j.semcdb.2013.04.001> (2013).
- 410 3 Cuthill, I. C. *et al.* The biology of color. *Science* **357**, doi:10.1126/science.aan0221 (2017).
- 411 4 Shawkey, M. D. & D'Alba, L. Interactions between colour-producing mechanisms and
412 their effects on the integumentary colour palette. *Philos Trans R Soc Lond B Biol Sci* **372**,
413 doi:10.1098/rstb.2016.0536 (2017).
- 414 5 Thayer, R. C., Allen, F. I. & Patel, N. H. Structural color in *Junonia* butterflies evolves by
415 tuning scale lamina thickness. *Elife* **9**, doi:10.7554/eLife.52187 (2020).
- 416 6 Kelsh, R. N., Harris, M. L., Colanesi, S. & Erickson, C. A. Stripes and belly-spots -- a review
417 of pigment cell morphogenesis in vertebrates. *Semin Cell Dev Biol* **20**, 90-104,
418 doi:10.1016/j.semcdb.2008.10.001 (2009).
- 419 7 Parichy, D. M. & Spiewak, J. E. Origins of adult pigmentation: diversity in pigment stem
420 cell lineages and implications for pattern evolution. *Pigment Cell Melanoma Res* **28**, 31-
421 50, doi:10.1111/pcmr.12332 (2015).
- 422 8 Nordlund, J. J., Abdel-Malek, Z. A., Boissy, R. E. & Rheins, L. A. Pigment Cell Biology: An
423 Historical Review. *Journal of Investigative Dermatology* **92**, S53-S60,
424 doi:<https://doi.org/10.1038/jid.1989.33> (1989).

- 425 9 Nordlund, J. J. *et al.* *The Pigmentary System: Physiology and Pathophysiology*. 2nd edn,
426 (Wiley, 2008).
- 427 10 Goda, M. & Fujii, R. The Blue Coloration of the Common Surgeonfish, *Paracanthurus*
428 *hepatus*-II. Color Revelation and Color Changes. *Zoolog Sci* **15**, 323-333,
429 doi:10.2108/zsj.15.323 (1998).
- 430 11 Frohnofer, H. G., Krauss, J., Maischein, H. M. & Nusslein-Volhard, C. Iridophores and
431 their interactions with other chromatophores are required for stripe formation in
432 zebrafish. *Development* **140**, 2997-3007, doi:10.1242/dev.096719 (2013).
- 433 12 Salis, P. *et al.* Developmental and comparative transcriptomic identification of
434 iridophore contribution to white barring in clownfish. *Pigment Cell Melanoma Res* **32**,
435 391-402, doi:10.1111/pcmr.12766 (2019).
- 436 13 Krauss, J. *et al.* Endothelin signalling in iridophore development and stripe pattern
437 formation of zebrafish. *Biol Open* **3**, 503-509, doi:10.1242/bio.20148441 (2014).
- 438 14 Kaelin, C. B. *et al.* Specifying and sustaining pigmentation patterns in domestic and wild
439 cats. *Science* **337**, 1536-1541, doi:10.1126/science.1220893 (2012).
- 440 15 Xiong, Z. *et al.* Draft genome of the leopard gecko, *Eublepharis macularius*. *GigaScience*
441 **5**, doi:10.1186/s13742-016-0151-4 (2016).
- 442 16 Wise, P. A. D., Vickaryous, M. K. & Russell, A. P. An Embryonic Staging Table for In Ovo
443 Development of *Eublepharis macularius*, the Leopard Gecko. *The Anatomical Record* **292**,
444 1198-1212, doi:10.1002/ar.20945 (2009).
- 445 17 McLean, K. E. & Vickaryous, M. K. A novel amniote model of epimorphic regeneration:
446 the leopard gecko, *Eublepharis macularius*. *BMC Developmental Biology* **11**, 50,
447 doi:10.1186/1471-213X-11-50 (2011).
- 448 18 Delorme, S. L., Lungu, I. M. & Vickaryous, M. K. Scar-Free Wound Healing and
449 Regeneration Following Tail Loss in the Leopard Gecko, *Eublepharis macularius*. *The*
450 *Anatomical Record* **295**, 1575-1595, doi:10.1002/ar.22490 (2012).
- 451 19 Szydłowski, P. *et al.* Iridophoroma associated with the Lemon Frost colour morph of the
452 leopard gecko (*Eublepharis macularius*). *Scientific Reports* **10**, 5734,
453 doi:10.1038/s41598-020-62828-9 (2020).
- 454 20 Bagnara, J. T. in *International Review of Cytology* Vol. 20 (eds G. H. Bourne & J. F.
455 Danielli) 173-205 (Academic Press, 1966).
- 456 21 Denefle, J. P. & Lechaire, J. P. Localization of pigment cells in cultured frog skin. *Am J*
457 *Anat* **188**, 212-220, doi:10.1002/aja.1001880210 (1990).
- 458 22 DeMartini, D. G., Krogstad, D. V. & Morse, D. E. Membrane invaginations facilitate
459 reversible water flux driving tunable iridescence in a dynamic biophotonic system. *Proc*
460 *Natl Acad Sci U S A* **110**, 2552-2556, doi:10.1073/pnas.1217260110 (2013).
- 461 23 Aramaki, T. & Kondo, S. Method for disarranging the pigment pattern of zebrafish by
462 optogenetics. *Developmental Biology* **460**, 12-19,
463 doi:<https://doi.org/10.1016/j.ydbio.2018.12.019> (2020).
- 464 24 Morrison, R. L. & Frost-Mason, S. K. Ultrastructural analysis of iridophore
465 organellogenesis in a lizard, *Sceloporus graciosus* (Reptilia: Phrynosomatidae). *J Morphol*
466 **209**, 229-239, doi:10.1002/jmor.1052090209 (1991).

- 467 25 Hillier, L. W. *et al.* Sequence and comparative analysis of the chicken genome provide
468 unique perspectives on vertebrate evolution. *Nature* **432**, 695-716,
469 doi:10.1038/nature03154 (2004).
- 470 26 Lander, E. S. *et al.* Initial sequencing and analysis of the human genome. *Nature* **409**,
471 860-921, doi:10.1038/35057062 (2001).
- 472 27 Kataoka, H., Kawaguchi, M., Fukushima, T. & Shimomura, T. Hepatocyte growth factor
473 activator inhibitors (HAI-1 and HAI-2): Emerging key players in epithelial integrity and
474 cancer. *Pathol Int* **68**, 145-158, doi:10.1111/pin.12647 (2018).
- 475 28 Kataoka, H. *et al.* Distribution of hepatocyte growth factor activator inhibitor type 1
476 (HAI-1) in human tissues. Cellular surface localization of HAI-1 in simple columnar
477 epithelium and its modulated expression in injured and regenerative tissues. *J*
478 *Histochem Cytochem* **47**, 673-682, doi:10.1177/002215549904700509 (1999).
- 479 29 Shimomura, T. *et al.* Hepatocyte growth factor activator inhibitor, a novel Kunitz-type
480 serine protease inhibitor. *J Biol Chem* **272**, 6370-6376, doi:10.1074/jbc.272.10.6370
481 (1997).
- 482 30 Gomez-Abenza, E. *et al.* Zebrafish modeling reveals that SPINT1 regulates the
483 aggressiveness of skin cutaneous melanoma and its crosstalk with tumor immune
484 microenvironment. *J Exp Clin Cancer Res* **38**, 405, doi:10.1186/s13046-019-1389-3
485 (2019).
- 486 31 Sakugawa, C. *et al.* Prognostic significance of hepatocyte growth factor activator
487 inhibitor type 1 (HAI-1) immunoreactivity in pancreatic ductal adenocarcinoma. *BMC*
488 *Res Notes* **10**, 674, doi:10.1186/s13104-017-3014-x (2017).
- 489 32 Baba, T. *et al.* Loss of membrane-bound serine protease inhibitor HAI-1 induces oral
490 squamous cell carcinoma cells' invasiveness. *J Pathol* **228**, 181-192,
491 doi:10.1002/path.3993 (2012).
- 492 33 Hoshiko, S. *et al.* Hepatocyte growth factor activator inhibitor type 1 is a suppressor of
493 intestinal tumorigenesis. *Cancer Res* **73**, 2659-2670, doi:10.1158/0008-5472.CAN-12-
494 3337 (2013).
- 495 34 Kawaguchi, M. *et al.* Membrane-bound serine protease inhibitor HAI-1 is required for
496 maintenance of intestinal epithelial integrity. *Am J Pathol* **179**, 1815-1826,
497 doi:10.1016/j.ajpath.2011.06.038 (2011).
- 498 35 Kawaguchi, M. *et al.* Inhibition of nuclear factor-kappaB signaling suppresses Spint1-
499 deletion-induced tumor susceptibility in the ApcMin/+ model. *Oncotarget* **7**, 68614-
500 68622, doi:10.18632/oncotarget.11863 (2016).
- 501 36 Carney, T. J. *et al.* Inactivation of serine protease Matriptase1a by its inhibitor Hai1 is
502 required for epithelial integrity of the zebrafish epidermis. *Development* **134**, 3461-3471,
503 doi:10.1242/dev.004556 (2007).
- 504 37 Fan, B. *et al.* Hepatocyte growth factor activator inhibitor-1 (HAI-1) is essential for the
505 integrity of basement membranes in the developing placental labyrinth. *Dev Biol* **303**,
506 222-230, doi:10.1016/j.ydbio.2006.11.005 (2007).
- 507 38 Cheng, H., Fukushima, T., Takahashi, N., Tanaka, H. & Kataoka, H. Hepatocyte growth
508 factor activator inhibitor type 1 regulates epithelial to mesenchymal transition through
509 membrane-bound serine proteinases. *Cancer Res* **69**, 1828-1835, doi:10.1158/0008-
510 5472.CAN-08-3728 (2009).

- 511 39 Tanaka, H. *et al.* Hepatocyte growth factor activator inhibitor type 1 (HAI-1) is required
512 for branching morphogenesis in the chorioallantoic placenta. *Mol Cell Biol* **25**, 5687-
513 5698, doi:10.1128/MCB.25.13.5687-5698.2005 (2005).
- 514 40 Nagaike, K. *et al.* Defect of hepatocyte growth factor activator inhibitor type 1/serine
515 protease inhibitor, Kunitz type 1 (Hai-1/Spint1) leads to ichthyosis-like condition and
516 abnormal hair development in mice. *Am J Pathol* **173**, 1464-1475,
517 doi:10.2353/ajpath.2008.071142 (2008).
- 518 41 Mathias, J. R. *et al.* Live imaging of chronic inflammation caused by mutation of
519 zebrafish Hai1. *J Cell Sci* **120**, 3372-3383, doi:10.1242/jcs.009159 (2007).
- 520 42 Kataoka, H. *et al.* Evaluation of hepatocyte growth factor activator inhibitor expression
521 in normal and malignant colonic mucosa. *Cancer Letters* **128**, 219-227,
522 doi:[https://doi.org/10.1016/S0304-3835\(98\)00067-6](https://doi.org/10.1016/S0304-3835(98)00067-6) (1998).
- 523 43 Ye, J. *et al.* Loss of hepatocyte growth factor activator inhibitor type 1 participates in
524 metastatic spreading of human pancreatic cancer cells in a mouse orthotopic
525 transplantation model. *Cancer Sci* **105**, 44-51, doi:10.1111/cas.12306 (2014).
- 526 44 Koivuniemi, R. *et al.* Hepatocyte growth factor activator inhibitor-1 is induced by bone
527 morphogenetic proteins and regulates proliferation and cell fate of neural progenitor
528 cells. *PLoS One* **8**, e56117, doi:10.1371/journal.pone.0056117 (2013).
- 529 45 List, K. *et al.* Deregulated matriptase causes ras-independent multistage carcinogenesis
530 and promotes ras-mediated malignant transformation. *Genes Dev* **19**, 1934-1950,
531 doi:10.1101/gad.1300705 (2005).
- 532 46 Olsson, M. *et al.* Mating system variation and morph fluctuations in a polymorphic lizard.
533 *Molecular Ecology* **16**, 5307-5315, doi:[https://doi.org/10.1111/j.1365-](https://doi.org/10.1111/j.1365-294X.2007.03578.x)
534 [294X.2007.03578.x](https://doi.org/10.1111/j.1365-294X.2007.03578.x) (2007).
- 535 47 Micheletti, S., Parra, E. & Routman, E. J. Adaptive Color Polymorphism and Unusually
536 High Local Genetic Diversity in the Side-Blotched Lizard, *Uta stansburiana*. *PLOS ONE* **7**,
537 e47694, doi:10.1371/journal.pone.0047694 (2012).
- 538 48 Rosenblum, E. B., Hoekstra, H. E. & Nachman, M. W. ADAPTIVE REPTILE COLOR
539 VARIATION AND THE EVOLUTION OF THE MC1R GENE. *Evolution* **58**, 1794-1808,
540 doi:<https://doi.org/10.1111/j.0014-3820.2004.tb00462.x> (2004).
- 541 49 Nunes, V. L., Miraldo, A., Beaumont, M. A., Butlin, R. K. & Paulo, O. S. Association of
542 Mc1r variants with ecologically relevant phenotypes in the European ocellated lizard,
543 *Lacerta lepida*. *Journal of Evolutionary Biology* **24**, 2289-2298,
544 doi:<https://doi.org/10.1111/j.1420-9101.2011.02359.x> (2011).
- 545 50 Fulgione, D., Lega, C., Trapanese, M. & Buglione, M. Genetic factors implied in melanin-
546 based coloration of the Italian wall lizard. *Journal of Zoology* **296**, 278-285,
547 doi:<https://doi.org/10.1111/jzo.12242> (2015).
- 548 51 Rosenblum, E. B., Römler, H., Schöneberg, T. & Hoekstra, H. E. Molecular and
549 functional basis of phenotypic convergence in white lizards at White Sands. *Proceedings*
550 *of the National Academy of Sciences* **107**, 2113, doi:10.1073/pnas.0911042107 (2010).
- 551 52 Laurent, S. *et al.* The population genomics of rapid adaptation: disentangling signatures
552 of selection and demography in white sands lizards. *Molecular Ecology* **25**, 306-323,
553 doi:<https://doi.org/10.1111/mec.13385> (2016).

- 554 53 Corso, J., Gonçalves, G. L. & Freitas, T. R. O. d. Sequence variation in the melanocortin-1
555 receptor (MC1R) pigmentation gene and its role in the cryptic coloration of two South
556 American sand lizards. *Genetics and Molecular Biology* **35**, 81-87 (2012).
- 557 54 Jin, Y. *et al.* Dorsal Pigmentation and Its Association with Functional Variation in MC1R in
558 a Lizard from Different Elevations on the Qinghai-Tibetan Plateau. *Genome Biology and*
559 *Evolution*, doi:10.1093/gbe/evaa225 (2020).
- 560 55 Rasys, A. M. *et al.* CRISPR-Cas9 Gene Editing in Lizards through Microinjection of
561 Unfertilized Oocytes. *Cell Rep* **28**, 2288-2292 e2283, doi:10.1016/j.celrep.2019.07.089
562 (2019).
- 563 56 Heckers, K. O., Aupperle, H., Schmidt, V. & Pees, M. Melanophoromas and
564 iridophoromas in reptiles. *J Comp Pathol* **146**, 258-268, doi:10.1016/j.jcpa.2011.07.003
565 (2012).
- 566 57 Rousselet, E. *et al.* Cutaneous iridophoroma in a Green iguana (*Iguana iguana*). *Vet Clin*
567 *Pathol* **46**, 625-628, doi:10.1111/vcp.12536 (2017).
- 568 58 Munoz-Gutierrez, J. F., Garner, M. M. & Kiupel, M. Cutaneous Chromatophoromas in
569 Captive Snakes. *Vet Pathol* **53**, 1213-1219, doi:10.1177/0300985816644302 (2016).
- 570 59 de Brot, S., Sydler, T., Nufer, L. & Ruetten, M. Histologic, Immunohistochemical, and
571 Electron Microscopic Characterization of a Malignant Iridophoroma in a Dwarf Bearded
572 Dragon (*Pogona Henrylawsoni*). *J Zoo Wildl Med* **46**, 583-587, doi:10.1638/2013-0113.1
573 (2015).
- 574 60 Bronson, E., Pereira, M., Sanchez, C. & Murray, S. Iridophoroma in a Veiled Chameleon,
575 *Chamaeleo calyptratus*. *Journal of Herpetological Medicine and Surgery* **16**, 58-60,
576 doi:10.5818/1529-9651.16.3.58 (2006).
- 577 61 Patterson, L. B. & Parichy, D. M. Interactions with iridophores and the tissue
578 environment required for patterning melanophores and xanthophores during zebrafish
579 adult pigment stripe formation. *PLoS Genet* **9**, e1003561,
580 doi:10.1371/journal.pgen.1003561 (2013).
- 581 62 Volkening, A. & Sandstede, B. Iridophores as a source of robustness in zebrafish stripes
582 and variability in *Danio* patterns. *Nat Commun* **9**, 3231, doi:10.1038/s41467-018-05629-
583 z (2018).
- 584 63 Hirata, M., Nakamura, K. & Kondo, S. Pigment cell distributions in different tissues of the
585 zebrafish, with special reference to the striped pigment pattern. *Dev Dyn* **234**, 293-300,
586 doi:10.1002/dvdy.20513 (2005).
- 587 64 Hirata, M., Nakamura, K., Kanemaru, T., Shibata, Y. & Kondo, S. Pigment cell
588 organization in the hypodermis of zebrafish. *Dev Dyn* **227**, 497-503,
589 doi:10.1002/dvdy.10334 (2003).
- 590 65 Singh, A. P., Schach, U. & Nusslein-Volhard, C. Proliferation, dispersal and patterned
591 aggregation of iridophores in the skin prefigure striped colouration of zebrafish. *Nat Cell*
592 *Biol* **16**, 607-614, doi:10.1038/ncb2955 (2014).
- 593 66 Krauss, J. *et al.* transparent, a gene affecting stripe formation in Zebrafish, encodes the
594 mitochondrial protein Mpv17 that is required for iridophore survival. *Biol Open* **2**, 703-
595 710, doi:10.1242/bio.20135132 (2013).

- 596 67 Fadeev, A., Krauss, J., Singh, A. P. & Nusslein-Volhard, C. Zebrafish Leucocyte tyrosine
597 kinase controls iridophore establishment, proliferation and survival. *Pigment Cell*
598 *Melanoma Res* **29**, 284-296, doi:10.1111/pcmr.12454 (2016).
- 599 68 Singh, A. P. & Nusslein-Volhard, C. Zebrafish stripes as a model for vertebrate colour
600 pattern formation. *Curr Biol* **25**, R81-R92, doi:10.1016/j.cub.2014.11.013 (2015).
- 601 69 Cooper, C. D. *et al.* Protein Kinase A Signaling Inhibits Iridophore Differentiation in
602 Zebrafish. *J Dev Biol* **6**, doi:10.3390/jdb6040023 (2018).
- 603 70 Irion, U. & Nusslein-Volhard, C. The identification of genes involved in the evolution of
604 color patterns in fish. *Curr Opin Genet Dev* **57**, 31-38, doi:10.1016/j.gde.2019.07.002
605 (2019).
- 606 71 Lewis, V. M. *et al.* Fate plasticity and reprogramming in genetically distinct populations
607 of Danio leucophores. *Proc Natl Acad Sci U S A* **116**, 11806-11811,
608 doi:10.1073/pnas.1901021116 (2019).
- 609 72 Masahito, P., Ishikawa, T. & Sugano, H. Pigment cells and pigment cell tumors in fish. *J*
610 *Invest Dermatol* **92**, 266S-270S, doi:10.1111/1523-1747.ep13076602 (1989).
- 611 73 Yang, K., Oak, A. S. W., Slominski, R. M., Brozyna, A. A. & Slominski, A. T. Current
612 Molecular Markers of Melanoma and Treatment Targets. *Int J Mol Sci* **21**,
613 doi:10.3390/ijms21103535 (2020).
- 614 74 Bayona-Vasquez, N. J. *et al.* Adapterama III: Quadruple-indexed, double/triple-enzyme
615 RADseq libraries (2RAD/3RAD). *PeerJ* **7**, e7724, doi:10.7717/peerj.7724 (2019).
- 616 75 Li, H. & Durbin, R. Fast and accurate short read alignment with Burrows-Wheeler
617 transform. *Bioinformatics* **25**, 1754-1760, doi:10.1093/bioinformatics/btp324 (2009).
- 618 76 McKenna, A. *et al.* The Genome Analysis Toolkit: a MapReduce framework for analyzing
619 next-generation DNA sequencing data. *Genome Res* **20**, 1297-1303,
620 doi:10.1101/gr.107524.110 (2010).
- 621 77 Catchen, J., Hohenlohe, P. A., Bassham, S., Amores, A. & Cresko, W. A. Stacks: an
622 analysis tool set for population genomics. *Mol Ecol* **22**, 3124-3140,
623 doi:10.1111/mec.12354 (2013).
- 624 78 Catchen, J. M., Amores, A., Hohenlohe, P., Cresko, W. & Postlethwait, J. H. Stacks:
625 building and genotyping Loci de novo from short-read sequences. *G3 (Bethesda)* **1**, 171-
626 182, doi:10.1534/g3.111.000240 (2011).
- 627 79 Danecek, P. *et al.* The variant call format and VCFtools. *Bioinformatics* **27**, 2156-2158,
628 doi:10.1093/bioinformatics/btr330 (2011).
- 629 80 Brooks, A. N. *et al.* Conservation of an RNA regulatory map between Drosophila and
630 mammals. *Genome Res* **21**, 193-202, doi:10.1101/gr.108662.110 (2011).
- 631 81 Pimentel, H., Bray, N. L., Puente, S., Melsted, P. & Pachter, L. Differential analysis of
632 RNA-seq incorporating quantification uncertainty. *Nat Methods* **14**, 687-690,
633 doi:10.1038/nmeth.4324 (2017).
- 634 82 Bray, N. L., Pimentel, H., Melsted, P. & Pachter, L. Near-optimal probabilistic RNA-seq
635 quantification. *Nat Biotechnol* **34**, 525-527, doi:10.1038/nbt.3519 (2016).
- 636 83 Endelman, J. B. Ridge Regression and Other Kernels for Genomic Selection with R
637 Package rrBLUP. *The Plant Genome* **4**, 250-255, doi:10.3835/plantgenome2011.08.0024
638 (2011).

639 84 Xavier, A., Xu, S., Muir, W. M. & Rainey, K. M. NAM: association studies in multiple
640 populations. *Bioinformatics* **31**, 3862-3864, doi:10.1093/bioinformatics/btv448 (2015).
641 85 Galwey, N. W. A new measure of the effective number of tests, a practical tool for
642 comparing families of non-independent significance tests. *Genet Epidemiol* **33**, 559-568,
643 doi:10.1002/gepi.20408 (2009).
644

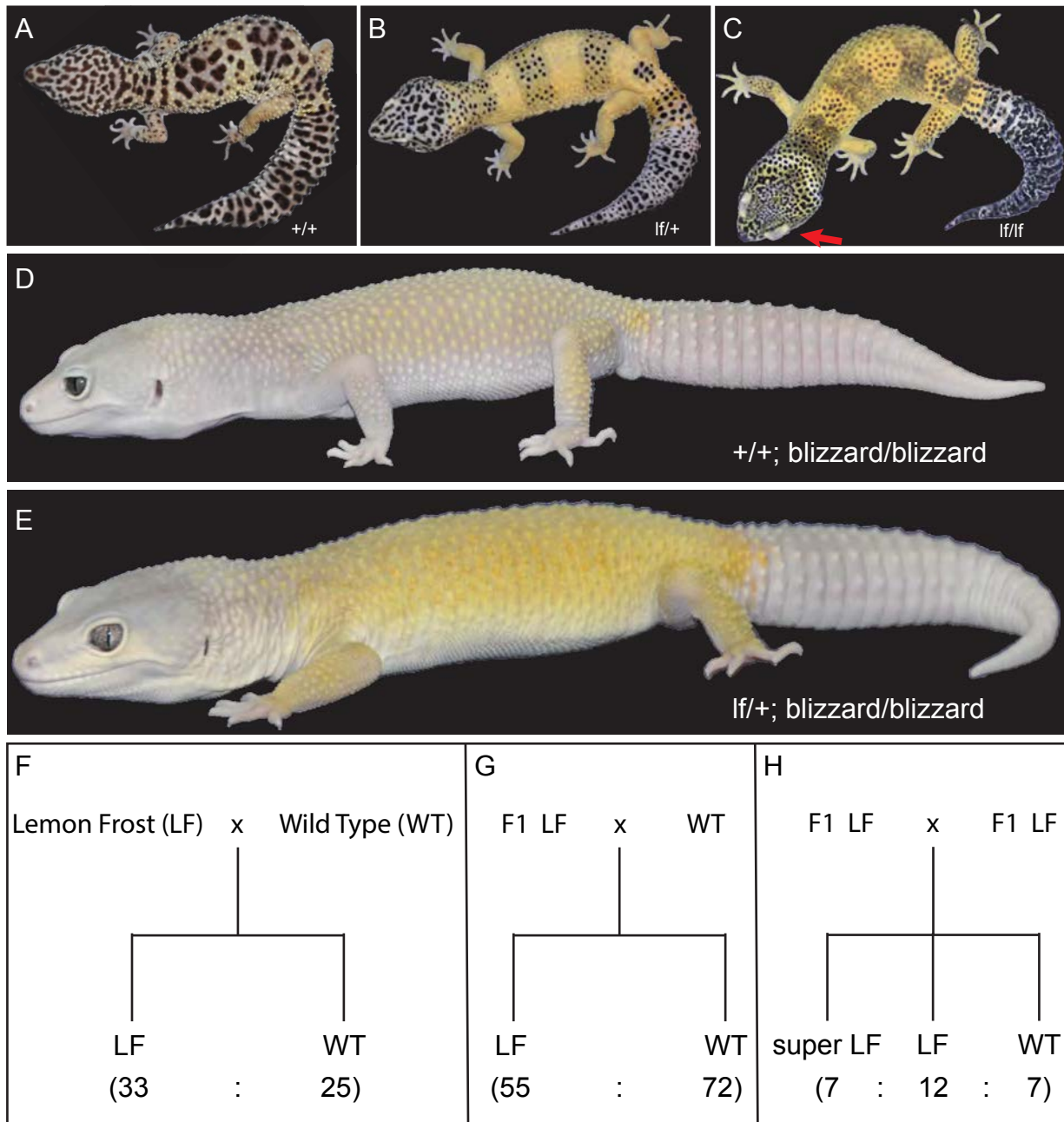


Fig 1 The Lemon Frost mutant of the common leopard gecko, *Eublepharis macularius*. (A) wild type; (B) heterozygous mutant; (C) homozygous mutant, with red arrow pointing to the eye lid; (D) blizzard mutant with minimal color; (E) Lemon Frost mutation (lf) on the blizzard background; (F-H) segregation of the lf allele. Lemon Frost (LF) denotes heterozygotes for the mutation; super LF denotes homozygotes for the mutation. All proportions are consistent with expectations for single-locus Mendelian inheritance (chi-square test $p > 0.1$).

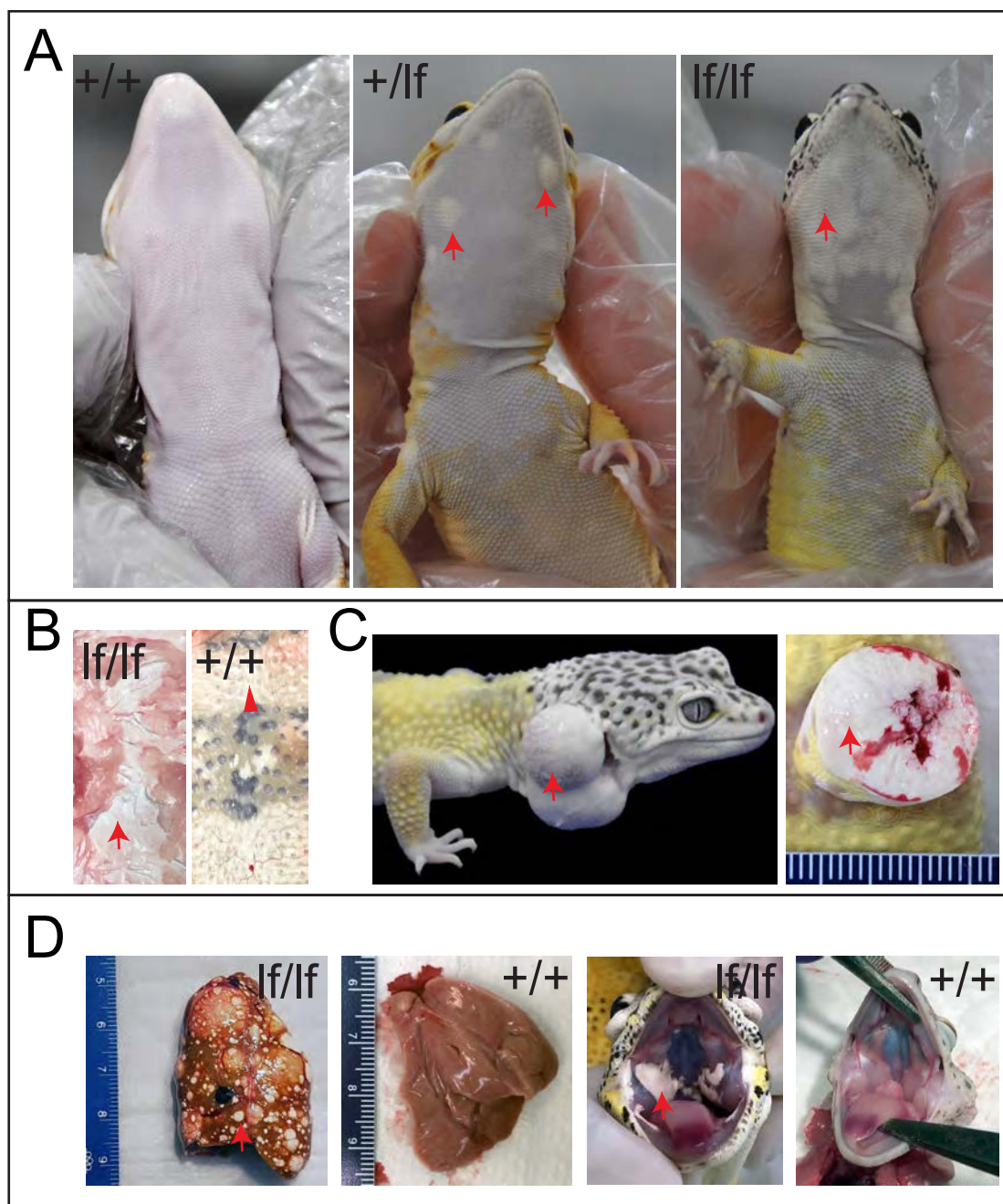


Fig 2 Tumor growth and metastasis in the Lemon Frost mutant. Designations are homozygous mutant (lf/lf); heterozygous mutant (lf/lf); wild type ($+/+$). (A) tumors in ventral skin; (B) thick layers of white tumor cells (lf/lf) vs. normal white cells ($+/+$); (C) outgrowth of white tumor cells (lf/lf); (D) metastasis of white tumor cells in the liver and oral cavity. Red arrows: white colored tumor cells. Arrowhead in B: normal white cells.

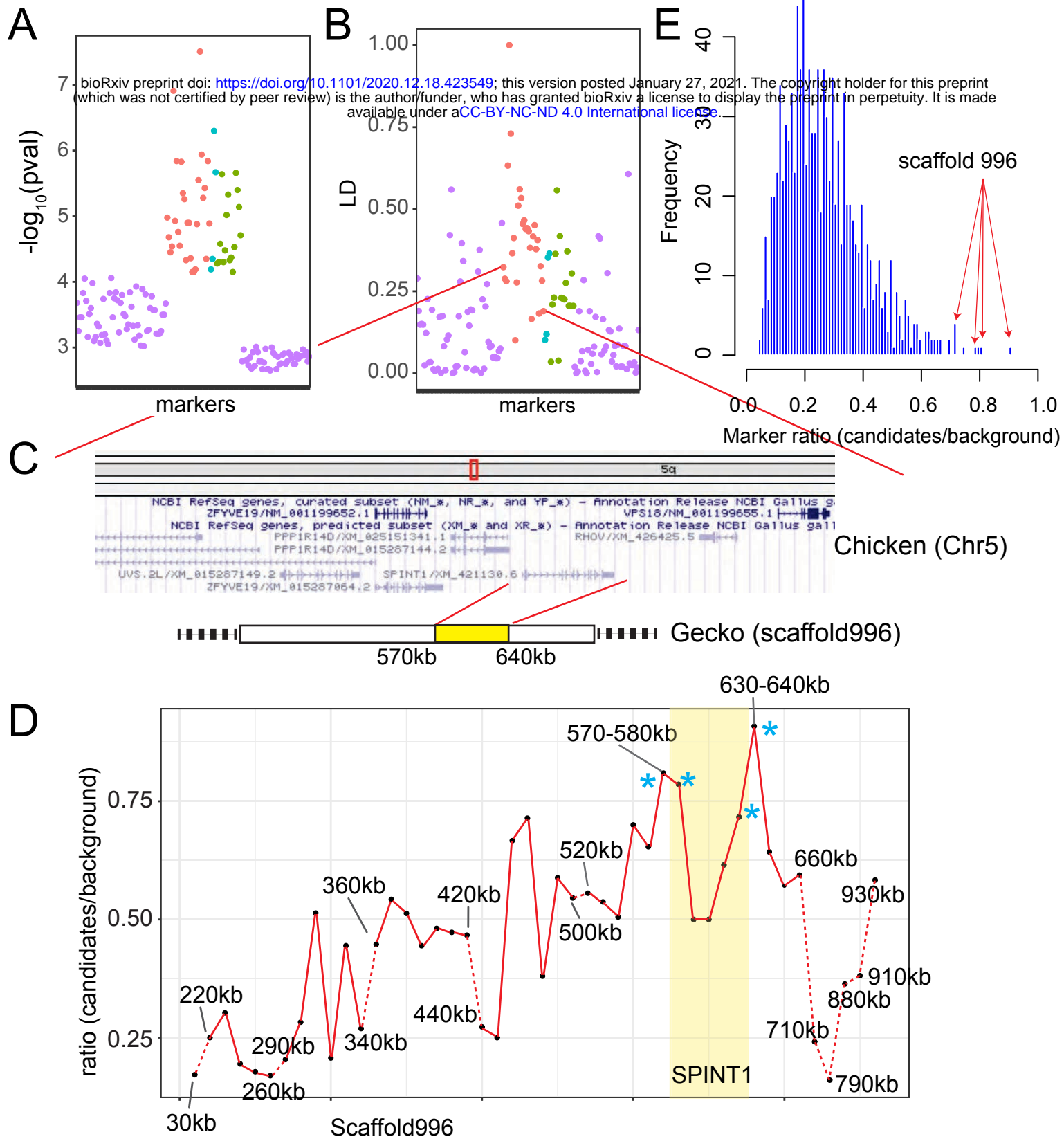


Fig 3 Localization of the Lemon Frost mutation. (A) p-value for association with white color and (B) linkage disequilibrium for 28 markers syntenic to chicken chromosome 1 (red, ordered by synteny), 4 markers syntenic to chromosome 5 (cyan), and 16 markers without synteny information (green). (C) A schematic of the region showing synteny and gene annotation. (D) Fraction of markers showing expected allele frequency pattern in pools, plotted for 10kb windows along scaffold 99. The four windows with the highest fraction are marked by asterisks and span the location of the gene SPINT1. Windows with fewer than 5 variants were not plotted (dashed red lines). (E) Genome-wide distribution of the fraction of markers showing expected allele frequency pattern in pools for all 10 kb windows. The 4 highest windows on scaffold 99 (red arrows) marked in D are among the 6 highest windows in the entire genome.

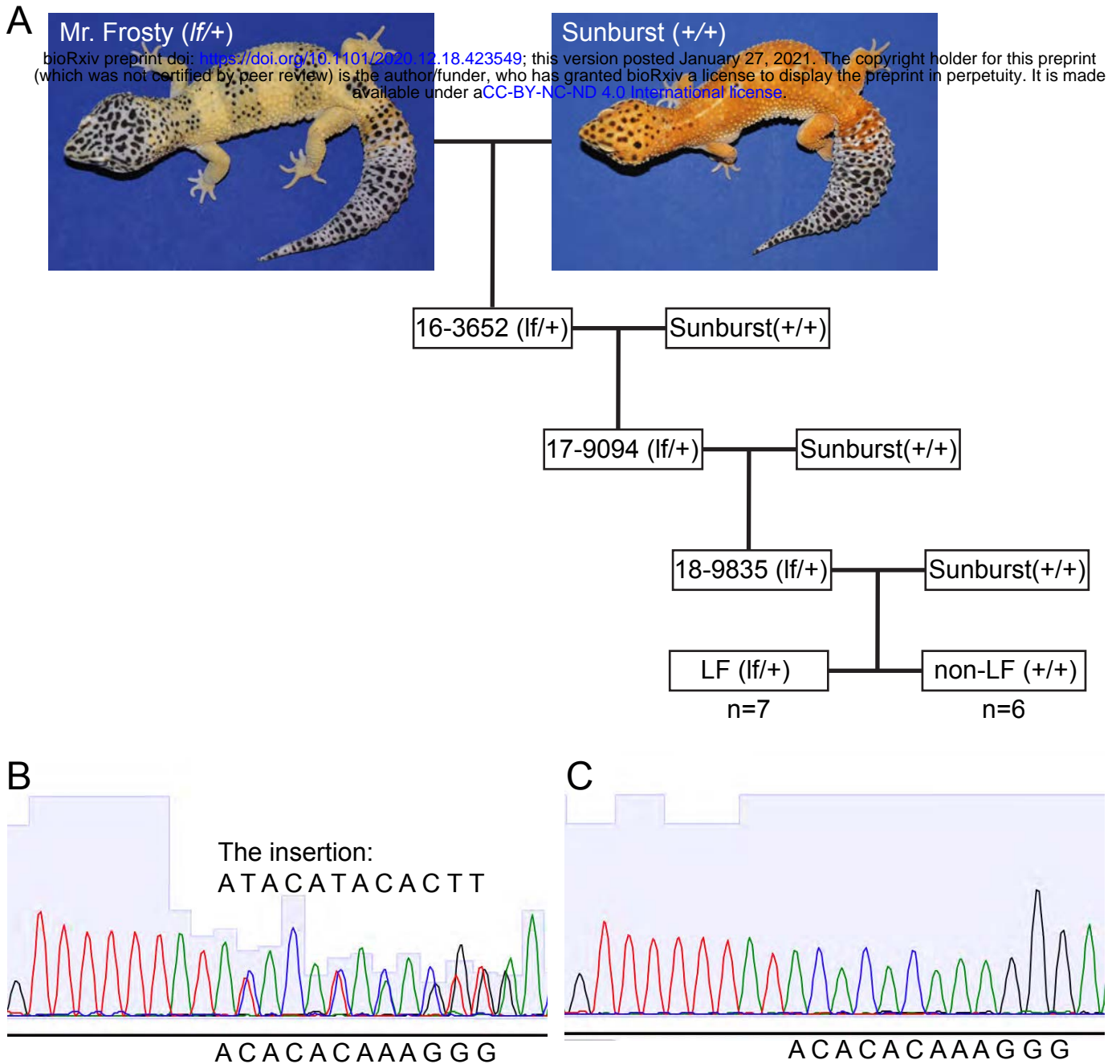
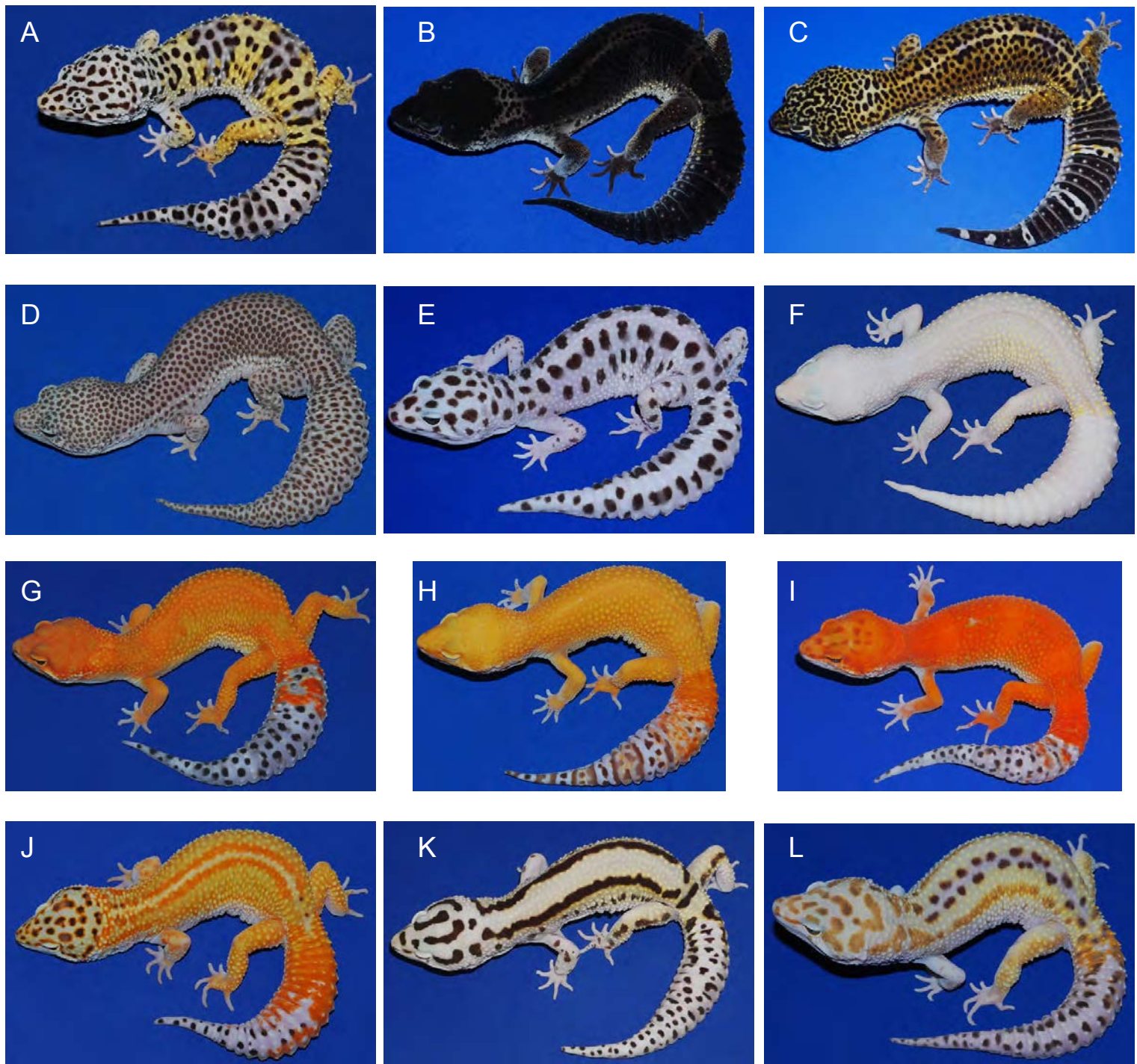
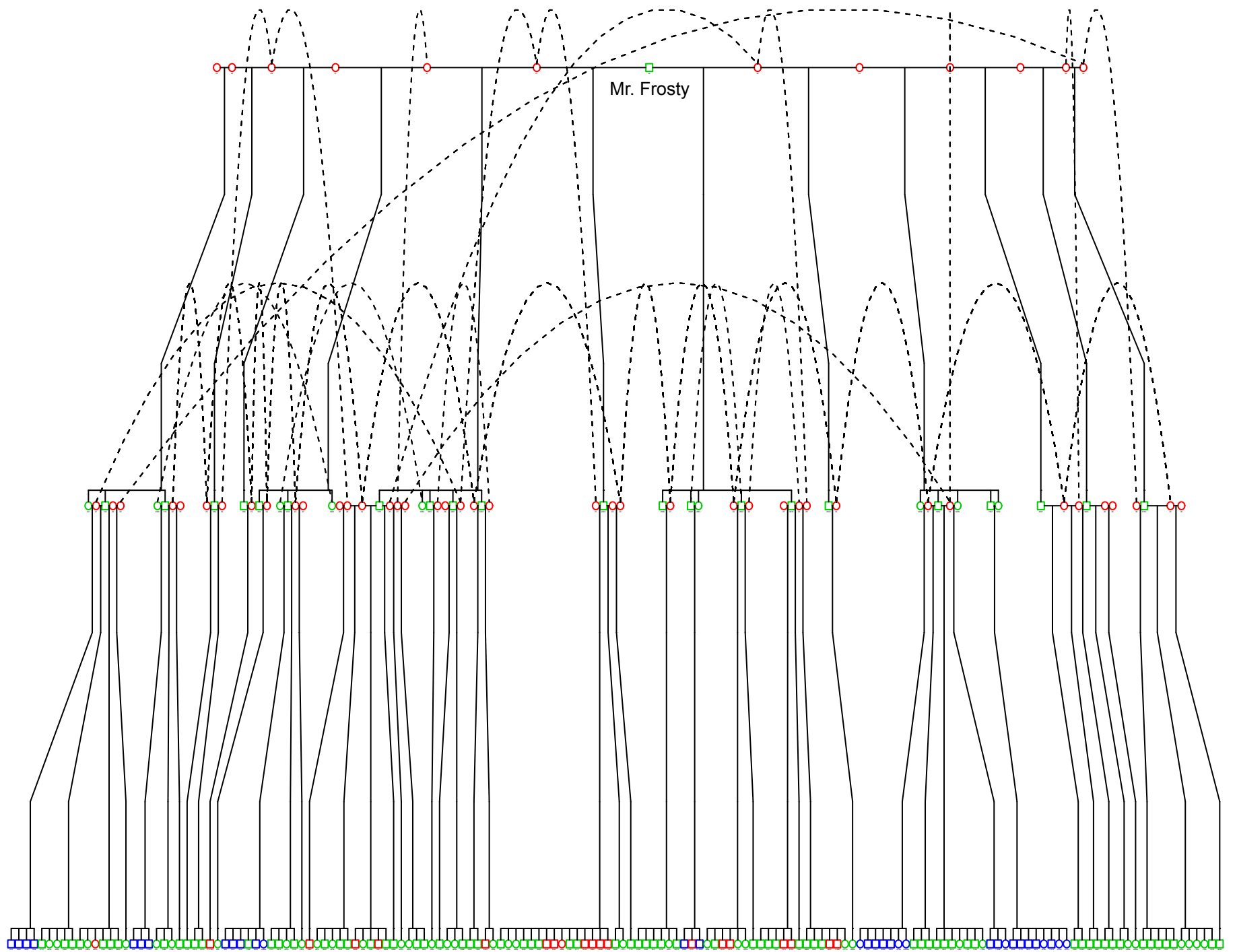


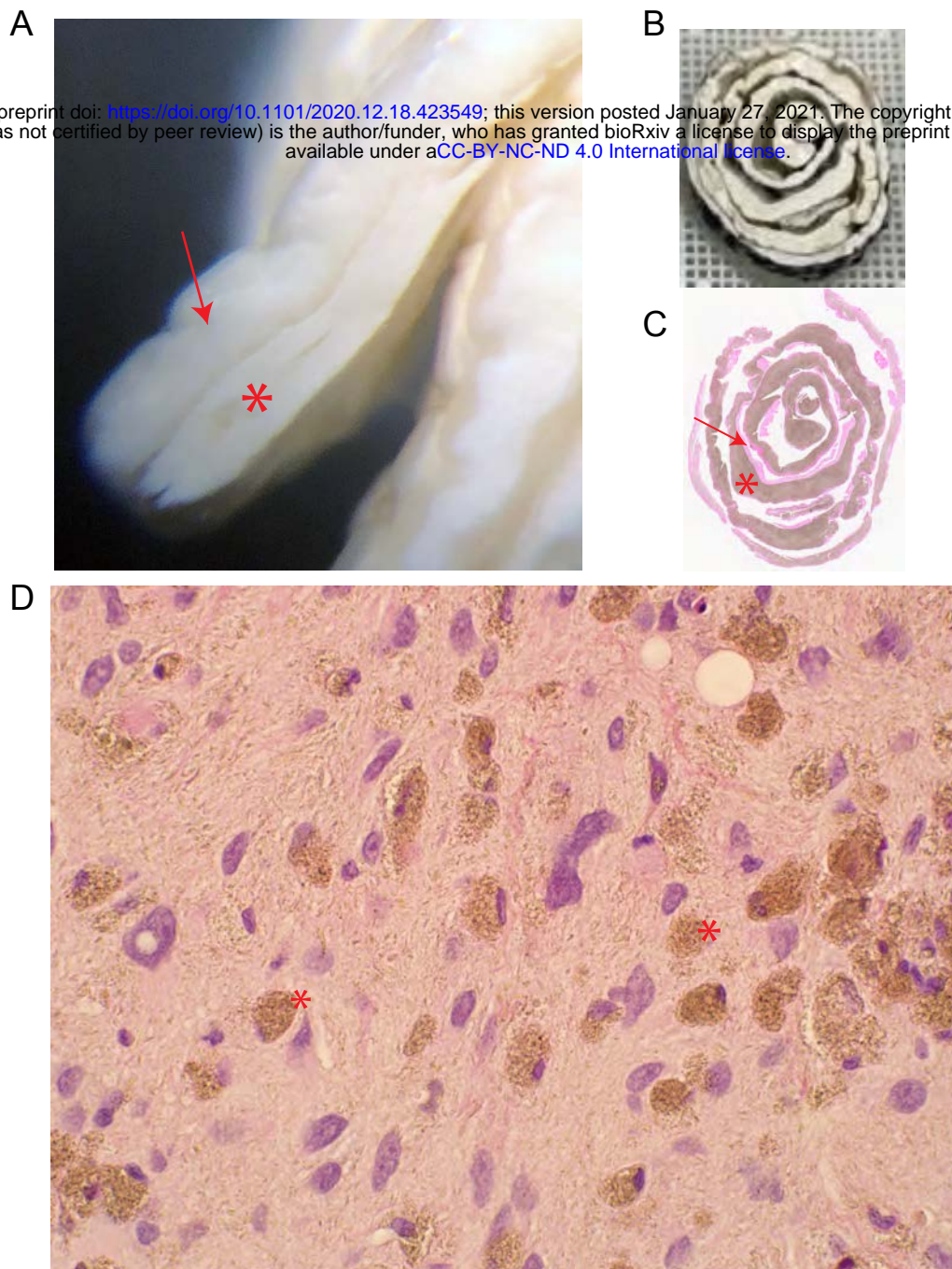
Fig The *lemon frost* allele in a backcross. (A) We genotyped 7 progeny with the Lemon Frost phenotype and 6 wild type progeny from the third generation of a backcross of Mr. Frosty to the Sunburst line for markers in the SPINT1 region and observed a consistent inheritance pattern. (B) Sequencing chromatogram of a heterozygous animal (*lf/+*) at an insertion marker. (C) Sequencing chromatogram of a homozygous animal (*+/+*) at the same insertion marker.



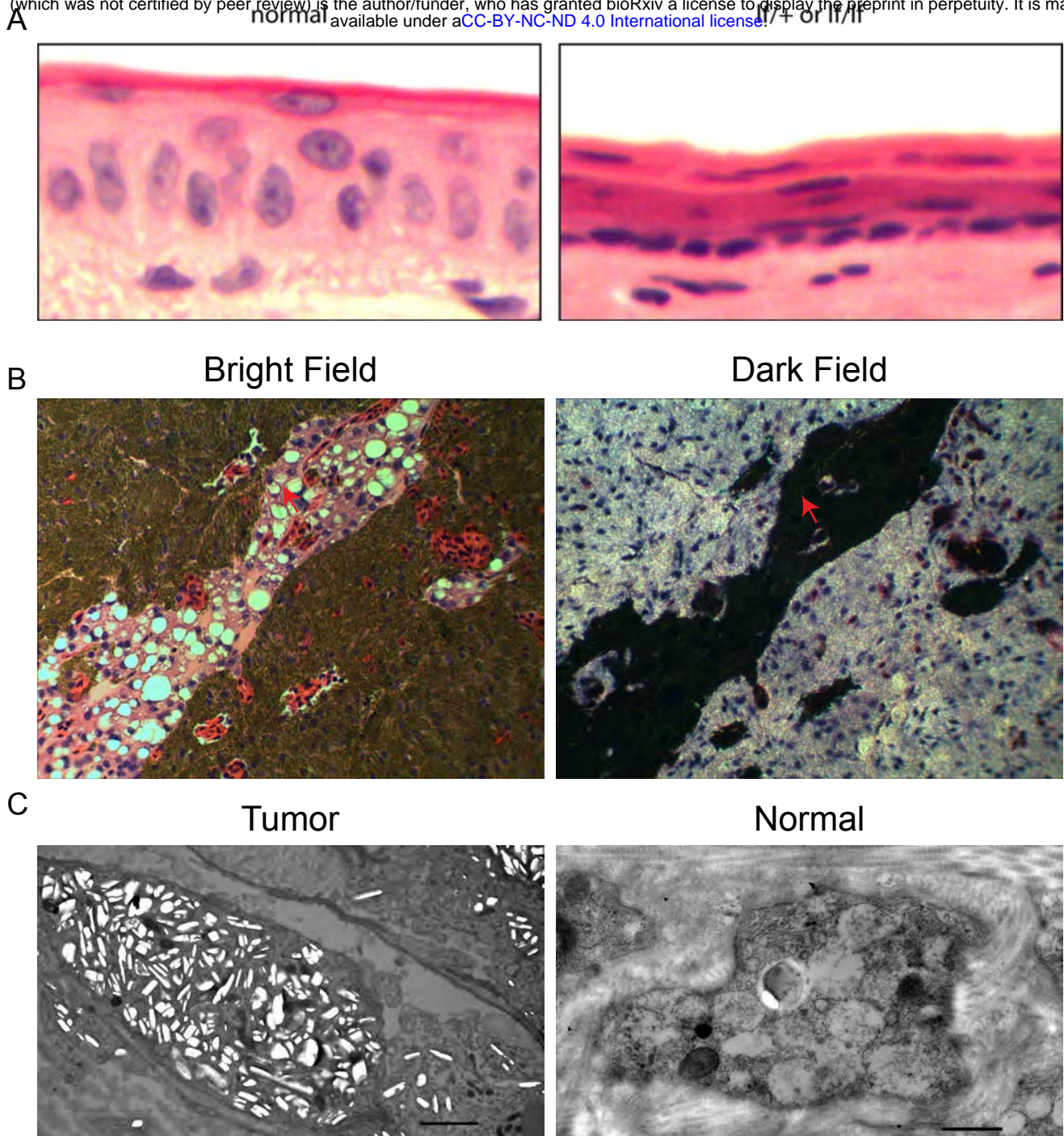
SupFig 1 Coloration and pattern diversity of the common leopard gecko, *Eublepharis macularius*. (A) wild type; (B) black night; (C) variant of black night; (D) granite snow; (E) gem snow; (F) white knight; (G) sunburst tangerine; (H-I) variants of sunburst tangerine; (J) red stripes; (K) bold stripes; (L) rainbow.



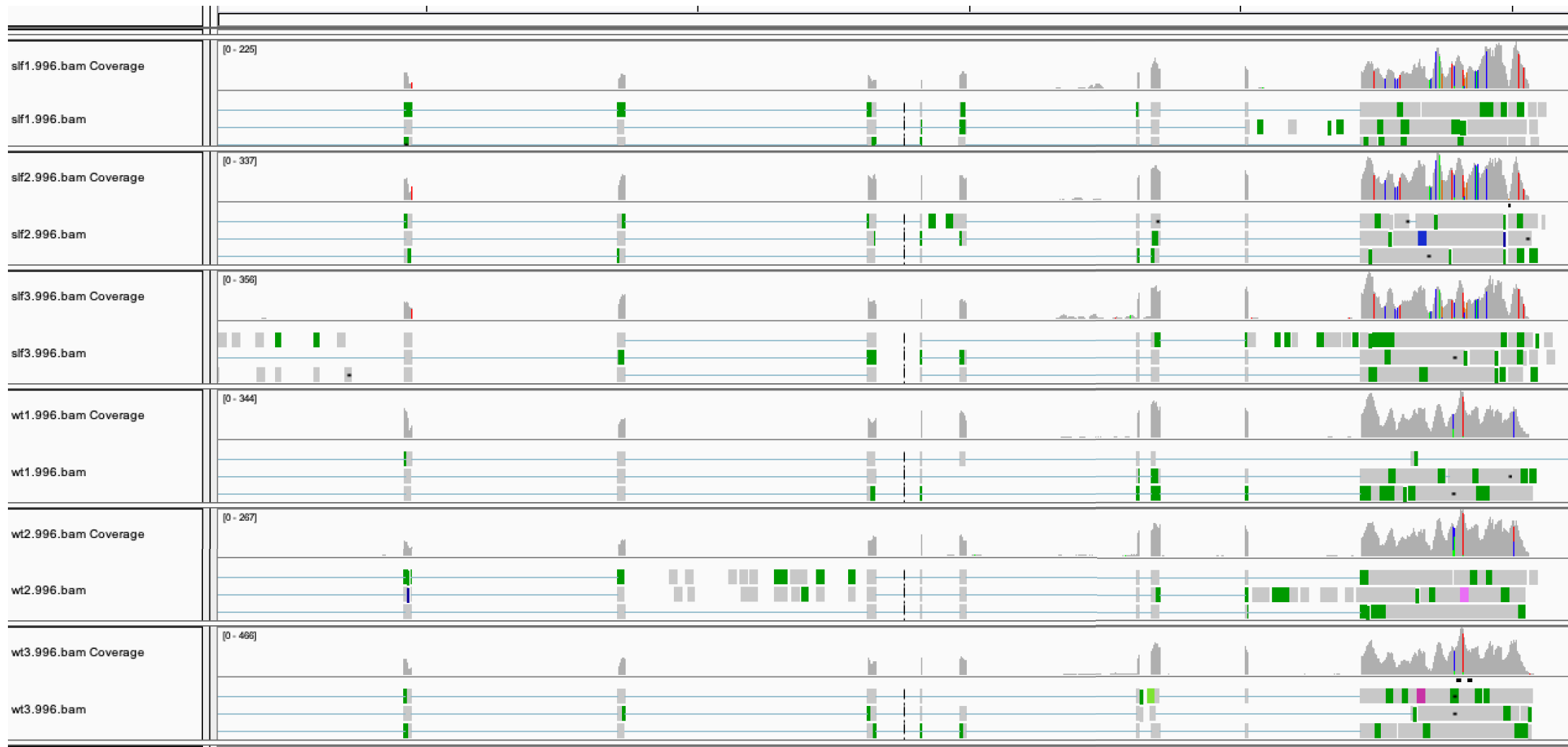
SupFig 2 Breeding pedigree of the Lemon Frost mutation. Mr. Frosty, the original carrier of the spontaneous Lemon Frost mutation, was bred to 12 female geckos from different genetic backgrounds. F1s carrying the *lf* allele were bred among themselves or back to their female parent, producing the second generation of animals heterozygous or homozygous for the *lf* allele. Blue: *lf/lf*; green: *lf/+*; red: *+/+*. Dashed line:



SupFig 3 Histopathology of skin tumors. (A) Thick layers of white tumor tissue (star) infiltrating white skin (arrow). (B) Skin biopsies organized and fixed in a paper roll for sectioning. (C) H&E staining of the skin sections. Arrow: skin; star: infiltrated tumor mass. (D) H&E staining of the skin sections showing normal skin cells and neoplastic cells (star). Neoplastic cells have eccentric and condensed nuclei.



SupFig 4 Potential metastasis of iridophoroma. (A) In normal skin, cell nuclei are oval and perpendicular to the skin surface. In Lemon Frost skin, cell nuclei are flat, elongated and parallel to the skin, reminiscent of epithelial-to-mesenchymal transition. (B) iridophoroma in the liver, stained dark in H&E sections. In dark field imaging, iridophores are bright white. Such iridophores invade blood vessels in the tissue (red arrows). (C) In TEM imaging, white tumor skins in super LF are filled with abundant iridophores with excessive brightly reflective crystals (Tumor). In normal skin, iridophores are much fewer and have less crystals (Normal).



SupFig 5 SPINT1 expression in gecko skin. SPINT1 mRNA reads from transcriptome sequencing were aligned to the genome and visualized in IGV. Top 3 rows show samples from homozygous mutants. Bottom rows show samples from wild type geckos. Skin tissue adjacent to the tumors was used in the mutants. Peaks mark SPINT1 exons. The last exon on the right is transcribed together with the 3'UTR.